Pergamon

Ocean Engineering 30 (2003) 387–400

OCEAN ENGINEERING

www.elsevier.com/locate/oceaneng

The coupled finite element and boundary element analysis of nonlinear interactions between waves and bodies

G.X. Wu [a,*], R. Eatock Taylor [b]

[a] *Department of Mechanical Engineering, University College London, Torrington Place, London WC1E 7JE, UK*

[b] *Department of Engineering Science, University of Oxford, Parks Road, Oxford OX1 3PJ, UK*

Received 2 October 2001; accepted 10 January 2002

Abstract

A coupled finite element (FEM) and boundary element (BEM) method is developed to analyse the nonlinear interaction between bodies and water waves. The former is used away from the body while the latter is used in a region near body. The combination is based on consideration of the efficiency of FEM and BEM in computation and mesh generation, respectively. Results for wave/body interactions are obtained by using auxiliary functions to decouple the mutual dependence of the body acceleration and the wave force.

Keywords: Nonlinear hydrodynamics; Boundary element method; Finite element method; Body responses

1. Introduction

The fully nonlinear wave/body interaction problem is usually solved by a time stepping technique based on potential flow theory. At each time step, the boundary value problem for the potential is commonly solved using the boundary element method (BEM) or the finite element method (FEM). The BEM divides only the boundary of the fluid domain into small panels. Early applications in the two dimen-

* Corresponding author. Tel.: +44-20-7679-3870; fax: +44-20-7388-0180..
E-mail address: gx_wu@meng.ucl.ac.uk (G.X. Wu).

0029-8018/02/$ - see front matter
PII: S0029-8018(02)00037-9

sional (2D) flow include work by Longuet-Higgins and Cokelet (1976); Faltinsen (1977); Vinje and Brevig (1981) and Lin et al. (1984). More recent applications to three dimensional (3D) flow include studies by Ferrant (1994) and Celebi et al. (1998). The FEM, on the other hand, divides the entire fluid domain into small elements. Typical applications to 2D flow include work by Wu and Eatock Taylor (1994, 1995); Clauss and Steinhagen (1999); Robertson and Sherwin (1999); and for 3D flow they include Wu et al. (1998) and Ma et al. (2001a, b).

As argued by Wu and Eatock Taylor (1995) and Ma et al. (2001a, b), although the BEM has far fewer unknowns, for the nonlinear wave/body interaction problem it usually requires much more memory because at each time step the unknowns are coupled by a fully populated matrix. By contrast, the FEM needs much less memory and is computationally far more efficient. A drawback of the FEM, however, is the mesh generation. For a complex structure, a sophisticated mesh generator is usually required to follow the motion of the body and the wave. Greaves et al. (1997) for example, adopted a quatree-based mesh generation scheme for the 2D problem. The scheme was found to be efficient when the horizontal and vertical dimensions of the fluid domain are comparable. For an extremely long or thin domain, the CPU requirement by the mesh generator increases rapidly. As remeshing is usually needed at every time step or after every few time steps, excessive CPU required by the mesh generator could make the overall computation very inefficient.

The present work therefore adopts the coupled BEM and FEM method. Near the body the BEM is used, as a boundary element mesh is easier to create. Also, when the BEM is confined to a small domain, its memory requirement is limited. Away from the body, the fluid domain will be regular if the wave does not overturn or break. This allows some simple mesh generator to be used, which can deal efficiently with a large, including extremely long or thin, fluid domain. The BEM and FEM adopted here are based on those in Wu and Eatock Taylor (1995). The additional work required is to ensure that the potential and velocity are continuous at the interface of the BEM and FEM domains. This is achieved through iteration, similar to that used by Wu and Eatock Taylor (1995) when implementing the domain decomposition method for the FEM.

2. Governing equations and boundary conditions

We consider the hydrodynamic problem of the interaction of a 2D body with waves generated by a piston-like wavemaker. A Cartesian coordinate system $O-xy$ is defined in which Oy coincides with the initial position of the wavemaker and points vertically upwards, and the origin O of the system is on the mean free surface. The physical parameters are nondimensionalised using the density of the fluid ρ and L, a typical dimension of the body. The time is nondimensionalised by $\sqrt{L/g}$, where g is the acceleration due to gravity. The fluid is assumed to incompressible and inviscid, and the flow is assumed to be irrotational. A velocity potential ϕ can then be introduced, which satisfies the Laplace equation

$$\nabla^2\phi = 0 \tag{1}$$

in the fluid domain R. On the body surface S_0, we have

$$\frac{\partial\phi}{\partial n} = (U-\Omega Y)n_x + (V + \Omega X)n_y, \tag{2}$$

where U and V are the translational velocities of the body in the x and y directions, respectively, $\vec{X} = (X,Y)$ are body-fixed coordinates relative to a point G in the body, Ω is the rotational velocity about G, and $\vec{n} = (n_x,n_y)$ is the normal vector on the body surface pointing out of the fluid domain. The other conditions on the rigid boundaries are on the bottom of the fluid S_B

$$\frac{\partial\phi}{\partial n} = 0, \tag{3}$$

and on the wavemaker S_W

$$\frac{\partial\phi}{\partial n} = U_0, \tag{4}$$

where U_0 is the velocity of the piston wavemaker. The kinematic and dynamic conditions on the free surface S_F ($y = \eta$) can be written as

$$\frac{\partial\phi}{\partial y} = \frac{\partial\eta}{\partial t} + \frac{\partial\phi\partial\eta}{\partial x\partial x}, \tag{5}$$

$$\eta + \frac{\partial\phi}{\partial t} + \frac{1}{2}\nabla\phi\nabla\phi = 0. \tag{6}$$

In the time stepping technique, the last two equations will give the potential on an updated free surface profile at the next time step, based on the solution at the current time step. The radiation condition used on the far right ($x\rightarrow\infty$) is the same as that in Ma et al. (2001a, b).

3. Coupled finite and boundary element method

As shown in Fig. 1, the fluid domain is divided into three regions. R_1 and R_3 are away from the body, where the FEM can be adopted as the mesh can be generated easily. R_2 encloses the body, where the BEM can be used. The continuity of the potential and the velocity is enforced on the two interfaces Γ_{12} and Γ_{23}.

Based on the FEM, the potential in R_1 can be written as

$$\phi^{(1)} = \sum_{j=1}^{n_1} \phi_j^{(1)} N_j(x,y) \tag{7}$$

where ϕ_j are the nodal values of the potential, n_1 is the number of the nodes in R_1 and $N_j(x,y)$ are the shape functions. In the present analysis these have been chosen

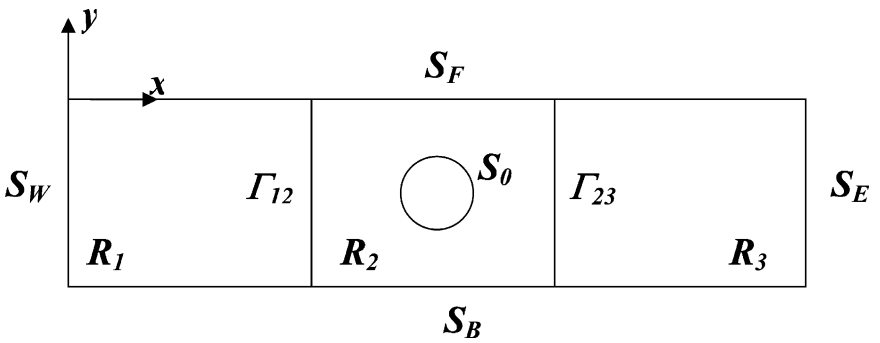

Fig. 1. The coupled FEM and BEM computational domain.

to be linear, based on triangular elements. Application of the Galerkin method within R_1 leads to

$$0 = \int_{R_1} \nabla^2 \phi^{(1)} N_i \mathrm{d}R = \int_{R_1} [\nabla(\nabla \phi^{(1)} N_i) - \nabla \phi^{(1)} \nabla N_i] \mathrm{d}R = \int_{S_1} N_i \frac{\partial \phi^{(1)}}{\partial n} \mathrm{d}S \tag{8}$$

$$- \int_{R_1} \nabla \phi^{(1)} \nabla N_i \mathrm{d}R$$

where S_1 is the boundary of R_1. Substituting Eq. (7) into Eq. (8) and using the boundary conditions, we obtain

$$\int_{R_1} \nabla N_i \sum_{j=1}^{n_1} \phi_j^{(1)} \nabla N_j \mathrm{d}R|_{j \notin S_{F_1}} = - \int_{R_1} \nabla N_i \sum_{j=1}^{n_1} \phi_j^{(1)} \nabla N_j \mathrm{d}R|_{j \in S_{F_1}} - U_0 \int_{S_W} N_i \mathrm{d}S \tag{9}$$

$$- \int_{\Gamma_{12}} \frac{\partial \phi^{(2)}}{\partial n} N_i \mathrm{d}S.$$

It should be noted that the direction of the normal on Γ_{12} changes sign from R_1 to R_2. S_{F_1} is the part of S_1 on the free surface (with analogous definitions used below for the boundaries to the regions R_2 and R_3).

Within R_2, the complex potential $\beta = \phi^{(2)} + \mathrm{i}\psi^{(2)}$ is defined, where $\psi^{(2)}$ is the stream function. Cauchy's theorem then gives

$$\oint \frac{\beta}{z - z_0} \mathrm{d}z = 0 \tag{10}$$

where $z = x + iy$ and z_0 is a point outside R_2. The integral in Eq. (10) is along the boundary of R_2, where we can write

$$\beta = \sum_{j=1}^{n_2} \beta_j N_j(z). \tag{11}$$

β_j are the values of the complex potential at n_2 nodes on the boundary, and the interpolation function is here chosen as

$$N_j(z) = \begin{cases} (z-z_{j+1})/(z-z_{j+1}) & z \in (z_j, z_{j+1}) \\ (z-z_{j-1})/(z-z_{j-1}) & z \in (z_{j-1}, z_j). \\ 0 \; z \notin (z_{j-1}, z_{j+1}) \end{cases} \tag{12}$$

Substituting Eq. (11) into Eq. (10), letting z_0 approach node z_k and using the boundary conditions, we have

$$\sum_{j=1}^{n_2} H_{kj}\phi_j^{(2)}\big|_{j\in S_0+S_{B_2}} + \mathrm{i}\sum_{j=1}^{n_2} H_{kj}\psi_j^{(2)}\big|_{j\in S_{F_2}+\Gamma_{12}+\Gamma_{13}} = -\sum_{j=1}^{n_2} H_{kj}\phi_j^{(2)}\big|_{j\in S_{F_2}} \tag{13}$$

$$-\sum_{j=1}^{n_2} H_{kj}\phi_j^{(2)}\big|_{j\in\Gamma_{12}} - \sum_{j=1}^{n_2} H_{kj}\phi_j^{(2)}\big|_{j\in\Gamma_{23}} - \mathrm{i}\sum_{j=1}^{n_2} H_{kj}\psi_j^{(2)}\big|_{j\in S_0+S_{B_2}},$$

where

$$H_{kj} = \frac{z_k - z_{j-1}}{z_j - z_{j-1}} \ln\frac{z_j - z_k}{z_{j-1} - z_k} + \frac{z_k - z_{j+1}}{z_j - z_{j-1}} \ln\frac{z_{j+1} - z_k}{z_j - z_k}. \tag{14}$$

In R_3, we can follow the procedure leading to Eq. (9). This gives the following equation for the potential $\phi^{(3)}$:

$$\int_{R_3} \nabla N_i \sum_{j=1}^{n_3} \phi_j^{(3)} \nabla N_j \mathrm{d}R\big|_{j\notin S_{F_3}+S_E} = -\int_{R_3} \nabla N_i \sum_{j=1}^{n_3} \phi_j^{(3)} \nabla N_j \mathrm{d}R\big|_{j\in S_{F_3}+S_E} - \int_{\Gamma_{23}} \frac{\partial\phi}{\partial n} N_i \mathrm{d}S. \tag{15}$$

Here the potential on the boundary at the far end S_E is assumed to be known, because it can be obtained through the solution at the last time step using the radiation condition (Ma et al., 2001a, b).

Eqs. (9), (13) and (15) can be solved iteratively. When $\partial\phi^{(2)}/\partial n$ in Eq. (9) is assumed known (e.g. zero for the first iteration), the equation becomes complete and can be solved. From the solution of $\phi^{(1)}$ we replace$\phi^{(2)}$ on Γ_{12} in Eq. (13) by $\phi^{(2)} + \gamma(\phi^{(1)} - \phi^{(2)})$, where γ is a relaxation coefficient. When $\phi^{(2)}$ on Γ_{23} is assumed known in Eq. (13), the equation can be solved to give $\partial\phi^{(2)}/\partial n$ on Γ_{23} through the derivative of the stream function along the boundary. Subsequently, Eq. (13) can be solved to give the new value of the potential on Γ_{23} through $\phi^{(2)} + \gamma(\phi^{(3)} - \phi^{(2)})$. The solution procedure then returns to R_1 and is repeated until the desired accuracy has been achieved.

4. Analysis of the motion of the body

When the potential has been found, the Bernoulli equation can be used to obtain the pressure:

$$p = -\frac{\partial \phi}{\partial t} - \frac{1}{2}\nabla\phi\nabla\phi - y. \tag{16}$$

(It should be noted that p is here nondimensionalised by ρgL, as discussed in the first paragraph of Section 2.) The hydrodynamic force and moment on the body can be obtained by integrating the pressure over its wetted surface:

$$\vec{F} = \int_{S_0} p\vec{n}\,\mathrm{d}S, \tag{17}$$

$$\vec{M} = \int_{S_0} p(\vec{X} \times \vec{n})\mathrm{d}S. \tag{18}$$

From Newton's law, we have

$$[M_\mathrm{b}][A] = [F_\mathrm{h}] + [F_\mathrm{e}], \tag{19}$$

where $[M_\mathrm{b}]$ is the nondimensionalised body mass matrix, $[A]$ is the acceleration column vector including translation and rotation, $[F_\mathrm{h}]$ is a column vector of the hydrodynamic force components and moment, and $[F_\mathrm{e}]$ represents the external force and moment.

In theory, once the potential has been found at each time step, Eq. (19) could be used to work out the acceleration of the body, which could then be used to obtain the new velocity and the new position of the body. The difficulty, however, is the $\phi_t = \partial\phi/\partial t$ term, which is still unknown. It could be obtained by numerical differentiation with respect to time using the potential at the last time step, but such a procedure is usually not accurate enough and may lead to instability. Another method of obtaining ϕ_t is to represent it as another boundary value problem. We notice that it satisfies the Laplace equation and the free surface boundary condition in Eq. (6). On the rigid boundaries we have (Wu, 1998)

$$\frac{\partial \phi_t}{\partial n} = (\dot{\vec{U}} + \dot{\vec{\Omega}} \times \vec{X}).\vec{n} - \vec{U}.\frac{\partial \nabla\phi}{\partial n} + \vec{\Omega}.\frac{\partial}{\partial n}[\vec{X} \times (\vec{U} - \nabla\phi)] \tag{20}$$

on S_0;

$$\frac{\partial \phi_t}{\partial n} = \dot{\vec{U}}_0\vec{n} - \vec{U}_0\frac{\partial \nabla\phi}{\partial n} \tag{21}$$

on S_w; and

$$\frac{\partial \phi_t}{\partial n} = 0 \tag{22}$$

on S_B. Here the dots over the velocities indicate the derivatives with respect to time.

If the acceleration of the body in Eq. (20) were known, ϕ_t could be solved in a manner similar to that used for the potential itself. The difficulty is, however, that the acceleration is not known before ϕ_t is found.

Here we adopt another approach, proposed by Wu and Eatock Taylor (1996), which has also been used by Kashiwagi (2000). We notice in Eqs. (17) and (18) that it is not ϕ_t itself which is needed but an integration over the body surface. We therefore introduce some auxiliary functions χ_i. We require these to satisfy the Laplace equation in the fluid domain, and the following boundary conditions:

$$\frac{\partial \chi_i}{\partial n} = n_i \tag{23}$$

on the body surface, and

$$\chi_i = 0 \tag{24}$$

on the free surface, where n_i are the components of $\vec{n}$ and $\vec{X} \times \vec{n}$, corresponding to those in Eqs. (17) and (18). On all other boundaries, we specify

$$\frac{\partial \chi_i}{\partial n} = 0. \tag{25}$$

Green's identity leads to

$$\int_S \left(\phi_t \frac{\partial \chi_i}{\partial n} - \chi_i \frac{\partial \phi_t}{\partial n} \right) \mathrm{d}S = 0, \tag{26}$$

where S is the boundary of the fluid domain. Using the boundary conditions for ϕ_t on the free surface in Eq. (6) and on the solid boundaries in Eqs. (20)–(22), and the boundary conditions for χ_i in Eqs. (23)–(25), we obtain

$$\int_{S_0} \phi_t n_i \mathrm{d}S = \int_{S_0} \chi_i \left\{ [\dot{\vec{U}} + \dot{\vec{\Omega}} \times \vec{X}].\vec{n} - \vec{U}.\frac{\partial \nabla \phi}{\partial n} + \vec{\Omega}.\frac{\partial}{\partial n}[\vec{X} \times (\vec{U} - \nabla \phi)] \right\} \mathrm{d}S \tag{27}$$

$$+ \int_{S_F} \left(\frac{1}{2} \nabla \phi \nabla \phi + y \right) \frac{\partial \chi_i}{\partial n} \mathrm{d}S + \int_{S_W} (-\dot{U}_0 + U_0 \phi_{xx}) \chi_i \mathrm{d}S.$$

Substituting Eq. (27) into Eq. (19), we obtain

$$([M_b] + [C])[A] = [Q] + [F_e] \tag{28}$$

where $[C]$ is a matrix whose coefficients are

$$C_{ij} = \int_{S_0} \chi_i n_j \mathrm{d}S; \tag{29}$$

and $[Q]$ is a column with

$$Q_i = -\int_{S_0}\chi_i\left\{-\vec{U}\frac{\partial\nabla\phi}{\partial n} + \vec{\Omega}\frac{\partial}{\partial n}[\vec{X}\times(\vec{U}-\nabla\phi)]\right\}\mathrm{d}_{S-}$$

$$\int_{S_F+S_0}\left(\tfrac{1}{2}\nabla\phi\nabla\phi + y\right)\frac{\partial\chi_i}{\partial n}\mathrm{d}S + \int_{S_W}(-\dot{U}_0 + U_0\phi_{xx})\chi_i\mathrm{d}S \tag{30}$$

$$= -\int_{S_0}\chi_i\{[-\vec{U} + \vec{\Omega}\times\vec{X}]\}\frac{\partial\nabla\phi}{\partial n} - \vec{n}(\vec{\Omega}\times\vec{U})\mathrm{d}S -$$

$$\int_{S_F+S_0}\left(\frac{1}{2}\nabla\phi\nabla\phi + y\right)\frac{\partial\chi_i}{\partial n}\mathrm{d}S + \int_{S_W}(-\dot{U}_0 + U_0\phi_{xx})\chi_i\mathrm{d}S.$$

Eq. (28) shows that the acceleration of the body can be obtained directly once the potential has been found. The introduction of the auxiliary functions χ_i does not lead to significant increase in the computational effort. They can be solved together with the potential itself, as they satisfy the same types of boundary condition.

There is a second derivative of the potential in Eq. (30), which is usually prone to numerical inaccuracy. To avoid that, we can use Stokes theorem on the closed boundary S_0

$$\int_{S_0}\frac{\partial\chi_i f}{\partial x_j}n_k\mathrm{d}S = \int_{S_0}\frac{\partial\chi_i f}{\partial x_k}n_j\mathrm{d}S$$

where x_j and n_j are components of $\vec{X}$ and $\vec{n}$, respectively. The equation is valid even for a floating body since $\chi_i = 0$ on the free surface. Taking $f = \phi_{x_j}$, we obtain

$$\int_{S_0}\chi_i\frac{\partial\nabla\phi}{\partial n}\mathrm{d}S = \int_{S_0}\left(\chi_i\frac{\partial\nabla\phi}{\partial n} - \chi_i\nabla^2\phi\vec{n}\right)\mathrm{d}S = \int_{S_0}\left((\nabla\chi_i\nabla\phi)\vec{n} - \nabla\chi_i\frac{\partial\phi}{\partial n}\right)\mathrm{d}S. \tag{31}$$

Substituting Eq. (31) into Eq. (30) we have

$$Q_i = \int_{S_0}\{\nabla\chi_i[(\vec{U} + \vec{\Omega}\times\vec{X})\cdot\vec{n}][\nabla\phi - (\vec{U} + \vec{\Omega}\times\vec{X})] + \chi_i(\vec{\Omega}\times\vec{U})\cdot\vec{n}\}\mathrm{d}S \tag{32}$$

$$-\int_{S_F+S_0}\left(\frac{1}{2}\nabla\phi\nabla\phi + y\right)\frac{\partial\chi_i}{\partial n}\mathrm{d}S + \int_{S_W}(-\dot{U}_0 + U_0\phi_{xx})\chi_i\mathrm{d}S.$$

It should be noted that the procedure derived in this section can also be used for the 3D problem.

5. Numerical results

It is often convenient to use a Lagrangian formulation to track the free surface elevation. The drawback of this method is that the mesh may become distorted due to the movement of the fluid particles, and thus may cause the calculation to break down. It is therefore quite common to adopt remeshing and interpolation during the calculation. A side effect of this, however, is that if remeshing is applied too often the fluid flow will lose a significant amount of energy through numerical dissipation.

Here we focus on simulating the response of a submerged body (although the coupled BEM and FEM method can of course also be used for a floating body). This allows us to use an Eulerian approach to tracking the free surface motion if the wave does not overturn or break. Let x' be measured from the wavemaker, which means $x = x' + \int_0^t U_0 dt$. We fix x' for each node on the free surface. Then the variation of the potential and the wave elevation with time on these nodes can be obtained from

$$\frac{\mathrm{D}}{\mathrm{D}t}\{\eta[x' + \int_0^t U_0 \mathrm{d}t, t]\} = U_0\eta_x + \eta_t \tag{33}$$

$$= \phi_y + (U_0 - \phi_x)\eta_x + \phi_y(U_0 - \phi_x)\eta_x - \eta,$$

$$\frac{\mathrm{D}}{\mathrm{D}t}\{\phi[x' + \int_0^t U_0 \mathrm{d}t, \eta, t]\} = U_0\phi_x + \phi_y\frac{\mathrm{D}\eta}{\mathrm{D}t} + \phi_t = U_0\phi_x + \frac{1}{2}(\phi_y^2 - \phi_x^2) \tag{34}$$

$$+ \phi_y(U_0 - \phi_x)\eta_x - \eta,$$

in which Eqs. (5) and (6) have been used.

There are few choices in the structure of the BEM mesh but there are many options for the FEM mesh. The latter may strongly affect the solution procedure and the quality of the results. In recent work, Robertson and Sherwin (1999) suggested that a poor mesh structure may lead to instability. They also demonstrated that the mesh shown in Fig. 2 can give stable and accurate results. Such a mesh is used in calculating the following results.

Fig. 3 shows results for a neutrally buoyant circular cylinder of radius r_0 (with $L = r_0$ used for nondimensionalisation). The cylinder is initially submerged at $f = 1.5r_0$, where f is the distance between the centre of the cylinder and the mean water surface. It is placed at $15r_0$ away from the mean position of the wavemaker, which undergoes the motion defined by $U_0 = \omega a \sin\omega t$. The dimensionless frequency is taken to be $\omega = 1$. The far end of the computational domain is $65r_0$ away from the cylinder, where a radiation condition together with a damping zone is imposed (Ma et al., 2001a, b). The water depth is chosen as $h = 4r_0$. It is assumed that there is no external force restraining the cylinder, and its motion is entirely due to the hydro-

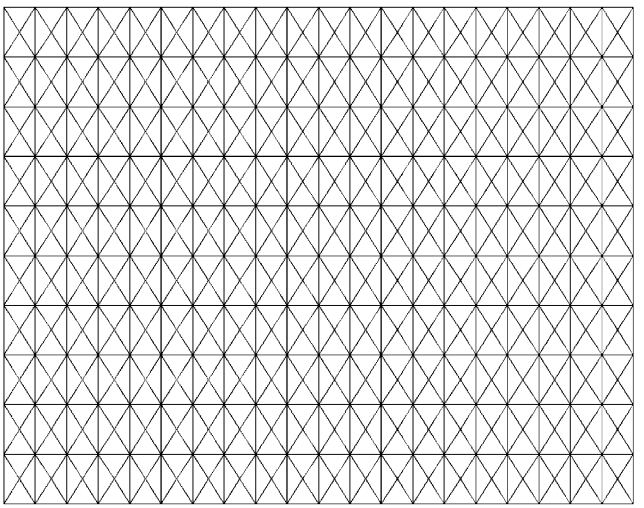

Fig. 2. The finite element mesh.

dynamic force. Figs. 3a-3d give results for displacement and total hydrodynamic force in the horizontal and vertical directions. They have been divided by the amplitude of the wavemaker motion a to highlight the nonlinear effect. The initial mesh used in the calculation has 80 elements on the body surface and has element size equal to $0.1r_0$ on the other boundaries. The dimensionless time step used is 0.01. These discretisation parameters have been found to give converged results. It can be seen that because there is no restoring force, the cylinder drifts away from its original position in the wave, the speed of the drift increasing with the amplitude of the wave maker motion. After taking up an offset down-wave during the first few cycles, the cylinder then drifts upwards and towards the wave maker. At this stage reflections back from the wave maker have started to influence the incoming wave field.

The circular cylinder is always a special case for fluid flow simulation. When, as here, the viscosity is ignored, there is no flow-induced moment to cause rotation about its centre. The results given above are therefore all related to translatory motion. We now consider an ellipse, to investigate rotation. All the parameters used in the calculation are the same as those for the circle, apart from the minor axis being taken as half the major axis. Also, to highlight the rotation, no translation is allowed in the simulation. Fig. 4 shows the calculated results. Their behaviour seems to be consistent with that in Fig. 3. The nonlinearity in the force in these cases is insignificant. Its main effect is on the drift motion. This can be partly explained by the fact that the body is fully submerged, and it is restrained from drifting towards the free surface (unlike the situation shown in Fig. 3).

To highlight the nonlinear effect, we next consider the case in which a circular cylinder is given a prescribed motion, but the wavemaker is stationary. Although the cylinder is submerged, nonlinear effects are expected to be more significant dur-

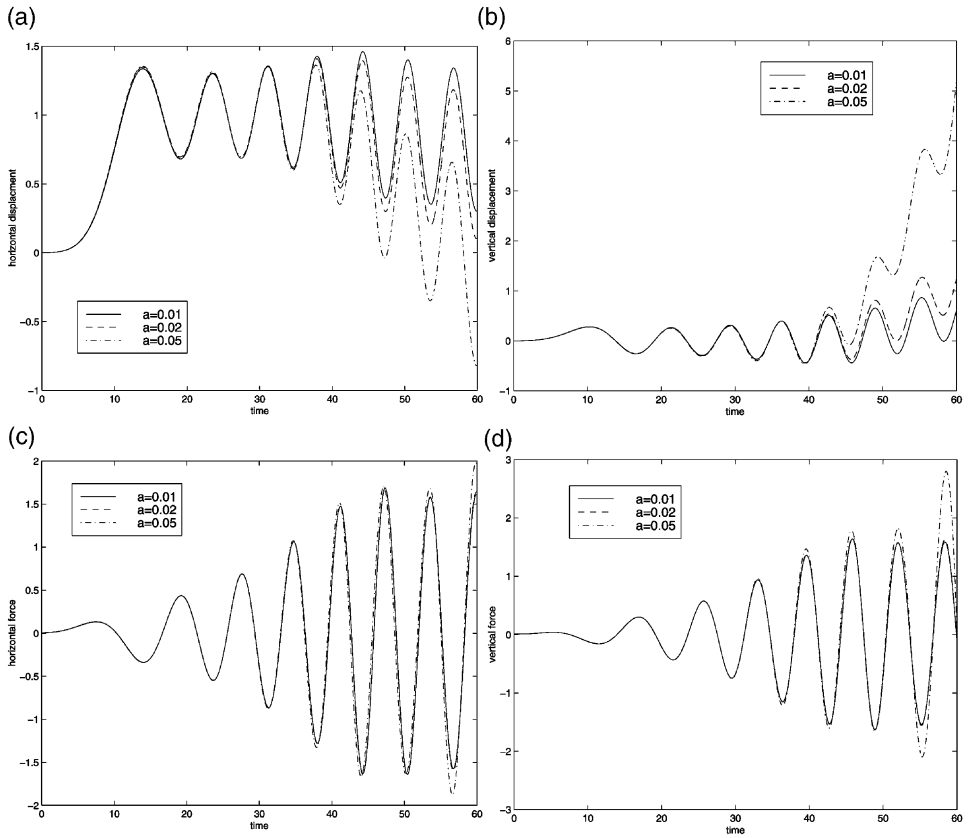

Fig. 3. Results for a submerged circular cylinder in the wave generated by a wavemaker: (a) horizontal displacement; (b) vertical displacement; (c) horizontal force; (d) vertical force.

ing the forced motion. The arrangement is the same as for the case leading to Fig. 3, except that the distance of the axis of the cylinder from each end of the tank is now $65r_0$. The motion of the cylinder is sinusoidal in the horizontal direction with $U = \omega a \sin\omega t$. The results given in Fig. 5 are have been divided by a and they correspond to $\omega = 1.0$. Based on the linear solution in the frequency domain, the vertical force would be zero because of anti-symmetry. The nonzero force shown in Fig. 5b is therefore due to the nonlinear effect. In particular, it has been shown by Wu (1993, 2000) that when the motion is periodic, the nonlinear vertical force has only components at $2n\omega$ while the horizontal force has only components at $(2n + 1)\omega, n = 0,1,2,\ldots$. This is seen to be consistent with the results in Fig. 5a and b.

6. Conclusions

A coupled FEM and BEM technique has been developed to analyse the nonlinear interactions between waves and bodies. It is based on the combination of the

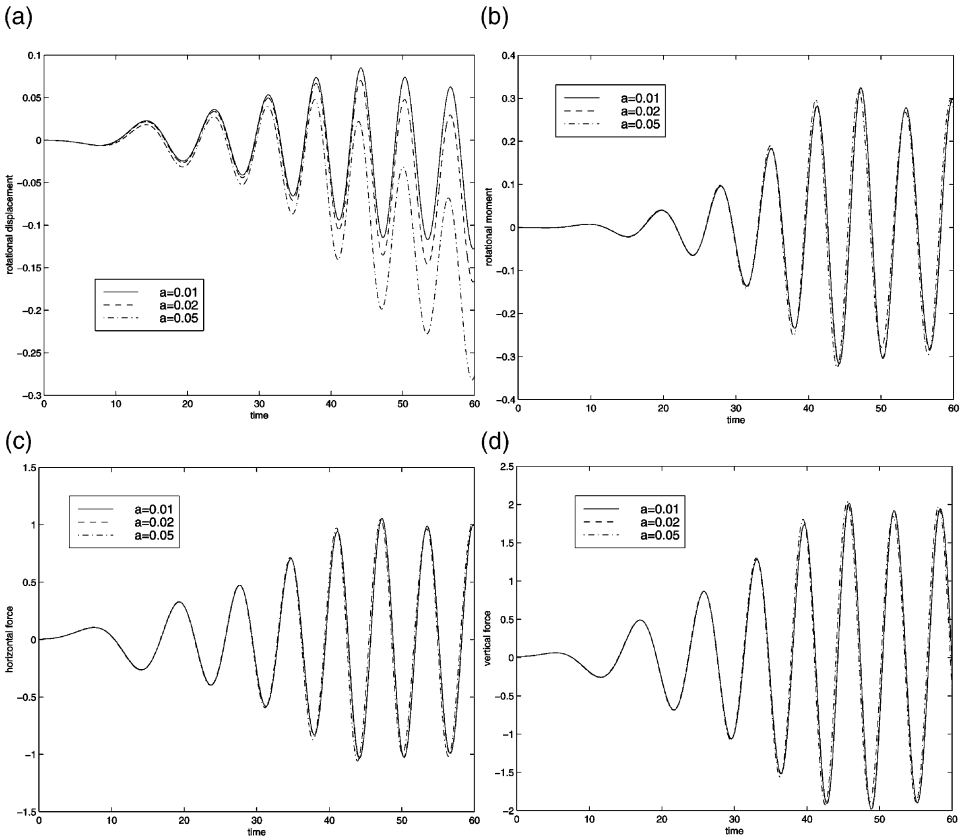

Fig. 4. Results for a submerged elliptical cylinder in the wave generated by a wavemaker: (a) rotational displacement (angle); (b) rotational moment; (c) horizontal force; (d) vertical force.

strengths of FEM and BEM in computational efficiency and in mesh generation respectively. Equations have also been derived to calculate the nonlinear motion of a body in waves, by introducing some auxiliary functions to decouple the mutual dependence of the body acceleration and the hydrodynamic forces. Some preliminary results have been provided to show the effectiveness of the developed techniques. These are for submerged bodies, thereby avoiding significant numerical dissipation when tracking the free surface. The method can however be used for more general cases, such as floating bodies and water entry and water exit problems. The experience here suggests that the technique has the potential to be used for complicated structures in steep waves. The penalty, however, when BEM is involved, is that the application is limited to the assumption of inviscid potential flow.

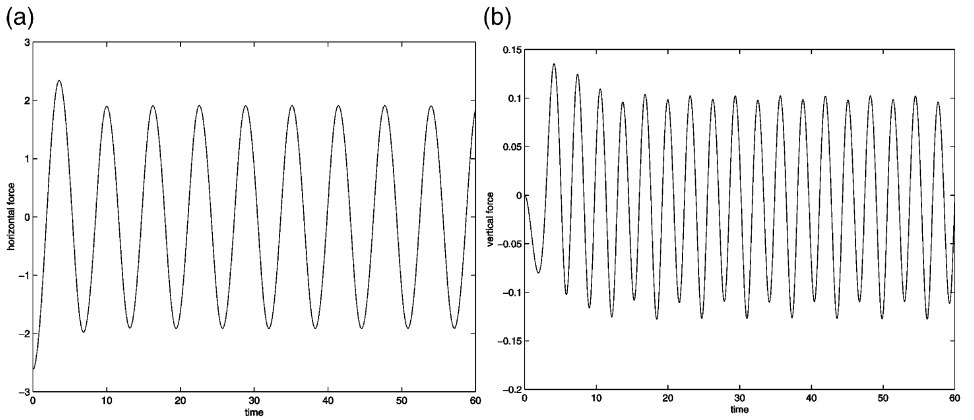

Fig. 5. Force on a submerged circular cylinder in forced sinusoidal horizontal motion: (a) horizontal force; (b) vertical force.

7. Acknowledgement

This work is supported by EPSRC through a joint project between UCL (GR/M57910) and Oxford (GR/M56401) for which the authors are most grateful.

References

Celebi, M.S., Kim, M.H., Beck, R.F., 1998. Fully nonlinear 3D numerical wave tank simulation. J. Ship Res. 42 (1), 33–45.

Clauss, G.F. , Steinhagen, U., 1999. Numerical simulation of nonlinear transient waves and its validation by laboratory data. In: Proc. 9th Int. Conf. Offshore and Polar Eng., Brest, France, Vol. 3. pp. 368–375.

Faltinsen, O.M., 1977. Numerical solution of transient nonlinear free surface motion outside or inside moving bodies. In: Proc. 2nd Int. Conf. on Numerical Ship Hydrodynamics, Berkeley, CA. pp. 347–357.

Ferrant, P., 1994. Radiation and diffraction of nonlinear waves in three dimensions. In: Proc. 7th Int. Conf. on Behaviour of Offshore Structures. MIT, USA, pp. 507–524.

Greaves, D.M., Borthwick, A.G.L., Wu, G.X., Eatock Taylor, R., 1997. A moving boundary finite element method for fully nonlinear wave simulation. J. Ship Res. 41, 181–194.

Kashiwagi, M., 2000. Nonlinear simulations of wave-induced motions of a floating body by means of the mixed Eulerian–Lagrangian method. Proc. Inst. Mech. Engrs. C 214, 841–855.

Lin, W.M., Newman, J.N., Yue, D.K. 1984. Nonlinear forced motion of floating bodies. Proc. 15th Symp. Naval Hydrodynamics, Hamburg, Germany. pp. 33–49.

Longuet-Higgins, M.S., Cokelet, E.D., 1976. The deformation of steep waves on water: I. a numerical method of computation. Proc. R. Soc. Lond. A 350, 1–26.

Ma, Q.W., Wu, G.X., Eatock Taylor, R., 2001a. Finite element simulation of fully nonlinear interaction between vertical cylinders and steep waves — part 1: methodology and numerical procedure. Int. J. Nume. Meth. Fluids 36, 265–285.

Ma, Q.W., Wu, G.X., Eatock Taylor, R., 2001b. Finite element simulation of fully nonlinear interaction between vertical cylinders and steep waves — part 2: numerical results and validation. Int. J. Nume. Meth. Fluids 36, 287–308.

Robertson, I., Sherwin, S., 1999. Free-surface flow simulation using hp/spectral elements. J. Comp. Phys. 155, 26–53.

Vinje, T., Brevig, P. 1981. Nonlinear ship motions. In: Proc. 3rd Int. Conf. on Numerical Ship Hydrodynamics, Paris, France. p. 257–268.

Wu, G.X., 1993. A note on hydrodynamic forces on body submerged below a free surface. Appl. Ocean Res. 15, 371–372.

Wu, G.X., 1998. Hydrodynamic force on a rigid body during impact with liquid. J. Fluids Structures 12, 549–559.

Wu, G.X., 2000. A note on non-linear hydrodynamic force on a floating body. Appl. Ocean Res. 22, 315–316.

Wu, G.X., Eatock Taylor, R., 1994. Finite element analysis of two dimensional non-linear transient water waves. Appl. Ocean Res. 16, 363–372.

Wu, G.X., Eatock Taylor, R., 1995. Time stepping solution of the two dimensional non-linear wave radiation problem. Ocean Eng. 22, 785–798.

Wu, G.X., Eatock Taylor, R., 1996. Transient motion of a floating body in steep waves. In: 11th Int Workshop on Water Waves and Floating Bodies, Hamburg.

Wu, G.X., Ma, Q.W., Eatock Taylor, R., 1998. Numerical simulation of sloshing waves in a 3D tank based on a finite element method. Appl. Ocean Res. 20, 337–355.